

A comparison of four turbulence models with an application to the West Pacific Warm Pool

AC. BENNIS*, M. GOMEZ MARMOL [†], R. LEWANDOWSKI [‡], T. CHACON REBOLLO [§] F. BROSSIER [¶]

Abstract

In this study, we compare four turbulence models usually used to parameterize the oceanic boundary layer. These four models depend on the bulk Richardson number, which is coherent with the studied region, the West Pacific Warm Pool, because of the large mean shear associated with the equatorial undercurrent. Two of these models, called R224 and R22, are new and the others are Pacanowski and Philander's model (R213 model) and Gent's model (R23 model). The numerical implementation is based on a non-conservative numerical scheme. The following (three criteria) are used to compare the models: the surface current intensity, the thermocline's form and the mixed layer depth. We start by a first series of numerical tests where the initial density and the initial velocity profiles are linear. This case aims valid our finite difference code and then to spotlight the four models behavior in this particular case. Next, we initialize the code with realistic velocity and density profiles thanks the TOGA-TAO array (McPhaden, 1995, [20]). In case of unstatic instability zone on the initial density profile, only the R224 model gives realistic results. Furthermore, we study the equilibrium solution. It is a linear solution which is in agreement with Bennis and al [1].

Summary 0.1 *Keywords: vertical mixing, Richardson number, mixing layer.*

1 Introduction

The presence of an homogeneous layer near the surface of the ocean has been observed since a long time. This layer presents almost constant profiles of temperature and salinity. We distinguish the mixing layer from the mixed layer (Brainerd and Gregg, 1995, [3]). The mixing layer is actively mixed by surface fluxes. It is a depth zone where the turbulence is strong. The mixed layer is a maximum depth zone which surface fluxes have been mixed in the recent

*IRMAR, Université de Rennes 1, Campus de Beaulieu, 35042 Rennes Cedex, France

[†]Departamento de Ecuaciones Diferenciales y Análisis Numerico, Universidad de Sevilla. C/Tarfia, s/n.41080, Sevilla, Spain

[‡]IRMAR, Université de Rennes 1, Campus de Beaulieu, 35042 Rennes Cedex, France

[§]Departamento de Ecuaciones Diferenciales y Análisis Numerico, Universidad de Sevilla. C/Tarfia, s/n.41080, Sevilla, Spain

[¶]IRMAR, Université de Rennes 1, Campus de Beaulieu, 35042 Rennes Cedex, France

past. This layer includes the mixing layer. The bottom of the mixed layer corresponds either to the top of the thermocline, zone of large gradients of temperature, or to the top of the zone where haline stratification is observed (Vialard and Delecluse, 1998, [30]). In this work, we study the mixed layer. The effect of the wind-stress acting on the sea-surface is considered to be the main forcing of this boundary layer. Observations in situ were completed by laboratory experiments (Deardoff, 1969, [4]) and more recently by numerical modelizations of the mixed layer. An historical of these different approaches can be found in Käse ([14]). Käse quoted the model of Kraus and Turner (1967, [15]) as the first applied mixed layer model. It is a bulk mixed-layer model. There are also first order models as the Pacanowski and Philander model (called PP model, 1981, [25]) and the Large and Gent model (called KPP model, 1994, [16]). The second order models have been developed by Mellor and Yamada (called MY model, 1982, [21]) and Gaspar and al (1990, [7]). In this work, we focus our attention on the first order models. According to observations, the thickness of the mixed layer can vary between ten meters and a few hundred of meters, depending on the latitude (Boyer de Montégut and al, 2004, [22]). The mixed layer depth is difficult to determine. Traditionally, there are two types of criteria for this determination: the density difference criterion which will be used in this work and the density gradient criterion. The first one consists in estimating the mixed layer depth as the depth where the density is about the surface density increased by 0.01 kg.m^{-3} . This criterion is often used in the tropical area as in Peters and al, 1988 [26]. So, the mixed layer is the layer where the density is inferior to the surface density to 0.01 kg.m^{-3} . The second criterion is based on specifying density gradient. The mixed layer depth is the depth where the density gradient is equal to the specified value.

Mixing processes are intense in the homogeneous boundary layer, much weaker near the thermocline or in the deep ocean. The effects of local fluxes of heat and momentum across the sea-surface induce turbulence and then mixing processes in the surface layer. The dynamical response of the ocean, and especially small scale turbulence, has a significant effect on mixing processes. This is true particularly in tropical areas. The rate of kinetic energy dissipation and the vertical turbulent fluxes of heat and mass cannot be measured directly, but they can be deduced from measurements of vertical temperature gradients and horizontal velocity [28]. Such experiments shown that turbulent dissipation is higher near the equator than in low latitudes [10], [11], [6]. Therefore in order to modelize the mixed boundary layer and to represent correctly the mixing processes, it is necessary to define a parametrization of turbulent diffusion. The mixed layer being strongly dominated by vertical fluxes, attention is focused on vertical mixing which requires a closure model in order to represent the Reynolds stress. Recently, Goosse et al. [9] studied the sensitivity of a global model to different parametrizations of vertical mixing. They insist on the crucial role of mixing in the upper oceanic layers: it has a direct impact on the sea surface temperature and then on ice evolution, but affects also the vertical profile of velocity by redistributing the momentum [2].

Classically, mixing parametrizations consist in the definition of turbulent eddy viscosity and

diffusivity coefficients. These coefficients can be chosen either as constants or as fixed profiles [13]. This is a simple but crude parametrization since variations of mixing with time and location are forbidden. A more suitable method is to define these coefficients as functions of processes governing the mixing. In tropical oceans vertical stratification and velocity shear are natural parameters since, following Philander [28], one of the reasons for higher turbulent dissipation near the equator than in low latitudes, is the large vertical shear observed in tropical currents. Pacanowski and Philander [25] proposed a formulation for eddy viscosity and diffusivity coefficients depending on the Richardson number which represents the ratio between buoyancy effects and vertical shear. The Richardson number dependent formulations allow strong mixing in high shear regions with low stratification, and low mixing elsewhere. It has to be noted that stratification tends to reduce turbulence and therefore mixing processes.

In this paper, we study first order models. We focus our attention on the behavior of Richardson number depending models: the basic one proposed by Pacanowski-Philander (PP model) and three variants used in Gent [8], Blanke and Delecluse [2], Goosse and al [9]. In this study, the PP model is called R213 model and the Gent model is called R23 model. The others models are named R224 and R22 models. The studied region is the West Pacific Warm Pool. At this location, the modelization based on the Richardson number is realistic because of the large mean shear associated with the equatorial undercurrent. Peters and al [26] have shown that the PP model underestimates the turbulent mixing at low Richardson number, while overestimating the turbulent mixing at high Richardson number in comparison with turbulent measurements. They found that the simulated thermocline is much too diffused compared with observations (the density gradient of simulated thermocline is weaker than the realistic density gradient). Furthermore, this scheme overestimates the surface current intensity and the simulated equatorial undercurrent is too shallow compared to observations ([12],[23],[18]). Halpern and al [12] compared the PP scheme and the MY scheme. At the equator, the current and temperature simulated by the PP scheme are more realistic than the current and temperature simulated by the Mellor and Yamada scheme. The Gent model, one of four studied models, gives realistic results in the West Pacific Warm Pool. It simulates a sharp thermocline which is in agreement with the observations [8]. This model gives good results for the annual average SST (Sea Surface Temperature) at the equator.

In this paper, we investigate in case of each model, the simulated mixed layer depth, the form of the simulated thermocline (sharp or diffuse) and the intensity of the simulated surface current. The numerical implementation is based on a non-conservative numerical scheme. We start by a first series of numerical tests where the initial density and the initial velocity profiles are linear. This case aims valid our finite difference code and then to spotlight the four models behavior in this particular case. Next, we initialize the code with realistic velocity and density profiles. These profiles come from the TOGA-TAO array (McPhaden, 1995, [20]). The geographic location is $0^{\circ}N, 165^{\circ}E$ which is in the West Pacific Warm Pool. In the first part, we simulate a long time case so as to study the equilibrium solution (Bennis and al [1]). In the second part,

we seek for if the four models behavior is similar to the linear case. At last, we investigate a case where there is a static instability zone on the initial density profile.

2 Modelization of the mixed layer

2.1 Setting of the problem

Variables used in this paper to describe the mixed layer are statistical means of the horizontal velocity and of the density denoted by (u, v, ρ) . In the ocean, the density is function of temperature and the salinity through a state equation. So, we consider the density as an idealized thermodynamic variable which is intended to represent temperature and salinity variations. The formation of the mixing layer is a response to sea-air interactions: wind-stress, solar heating, precipitations or evaporation acting on the sea surface. The variability of temperature is considered as essential to understand the response of the ocean. For example, the existence of a sharp thermocline is a well known feature of the tropical areas. The thermal inertia of the water column is linked with the depth of the thermocline, which influences the sea-surface temperature. The role of the haline stratification, sometimes considered as less important, has been recently evidenced by Vialard and Delecluse [30]: a numerical modelization of the tropical Pacific produces a "barrier layer" depending on surface forcings and large scale circulation. The term "barrier layer" refers to the water column located between the bottom of the mixed layer and the top of the thermocline. It is present when the isohaline layer is shallower than the isothermal layer and then the depth of the mixed layer is controlled by the salinity.

The model studied hereafter is not expected to describe all the phenomena occurring in the mixed layer. Its purpose is only a better understanding of a classical closure model. Therefore we shall use simplified equations governing the variables u (zonal velocity), v (meridian velocity) and ρ (density).

The mixing layer being strongly dominated by vertical fluxes, we shall suppose that u, v and ρ are horizontally homogeneous and we so obtain a one-dimensional modelization. The Coriolis force will be neglected, which is valid in tropical oceans. Therefore, the equations governing the mixing layer are

$$\left\{ \begin{array}{l} \frac{\partial u}{\partial t} = -\frac{\partial}{\partial z} \langle u' w' \rangle, \\ \frac{\partial v}{\partial t} = -\frac{\partial}{\partial z} \langle v' w' \rangle, \\ \frac{\partial \rho}{\partial t} = -\frac{\partial}{\partial z} \langle \rho' w' \rangle, \end{array} \right. \quad (1)$$

where u', v', w', ρ' represent the fluctuations of the horizontal velocity, vertical velocity and the density. The notation $\langle \cdot \rangle$ signifies that the quantity is statistically averaged. Equations (1) are the classical equations corresponding to a modelization of a water column. Such equations can be found in [17] as the equations of the boundary layer. Equations (1) are not closed and then the vertical fluxes appearing in the right-hand size have to be modeled.

We study in this paper the behavior of a very classical closure modelization that uses the concept of eddy coefficients in order to represent turbulent fluxes. So we set

$$\begin{aligned}-\langle u' w' \rangle &= \nu_1 \frac{\partial u}{\partial z}, \\ -\langle v' w' \rangle &= \nu_1 \frac{\partial v}{\partial z}, \\ -\langle \rho' w' \rangle &= \nu_2 \frac{\partial \rho}{\partial z}.\end{aligned}$$

Coefficients ν_1 and ν_2 are called vertical eddy viscosity and diffusivity coefficients and will be expressed as functions of the Richardson number R defined as

$$R = -\frac{g}{\rho_0} \frac{\frac{\partial \rho}{\partial z}}{\left(\frac{\partial u}{\partial z}\right)^2 + \left(\frac{\partial v}{\partial z}\right)^2},$$

where g is the gravitational acceleration and ρ_0 a reference density (for example $\rho_0 = 1025 \text{ kg.m}^{-3}$). The set of equations, initial and boundary conditions governing the mixing layer can now be written

$$\left\{ \begin{array}{l} \frac{\partial u}{\partial t} - \frac{\partial}{\partial z} \left(\nu_1 \frac{\partial u}{\partial z} \right) = 0, \\ \frac{\partial v}{\partial t} - \frac{\partial}{\partial z} \left(\nu_1 \frac{\partial v}{\partial z} \right) = 0, \\ \frac{\partial \rho}{\partial t} - \frac{\partial}{\partial z} \left(\nu_2 \frac{\partial \rho}{\partial z} \right) = 0, \text{ for } t \geq 0 \text{ and } -h \leq z \leq 0, \\ u = u_b, v = v_b, \rho = \rho_b \text{ at the depth } z = -h, \\ \nu_1 \frac{\partial u}{\partial z} = \frac{\rho_a}{\rho_0} V_x, \nu_1 \frac{\partial v}{\partial z} = \frac{\rho_a}{\rho_0} V_y, \nu_2 \frac{\partial \rho}{\partial z} = Q \text{ at the surface } z = 0, \\ u = u_0, v = v_0, \rho = \rho_0 \text{ at initial time } t = 0. \end{array} \right. \quad (2)$$

In system (2), the constant h denotes the thickness of the studied layer that must contain the mixing layer. Therefore the circulation for $z < -h$, under the boundary layer, is supposed to be known, either by observations or by a deep circulation numerical model. This justifies the choice of Dirichlet boundary conditions at $z = -h$, u_b , v_b and ρ_b being the values of horizontal velocity and density in the layer located below the mixed layer. The air-sea interactions are represented by the fluxes at the sea-surface: V_x and V_y are respectively the forcing exerted by the zonal wind-stress and the meridional wind-stress and Q represents the thermodynamical fluxes, heating or cooling, precipitations or evaporation. We have $V_x = C_D |u^a|^2$ and $V_y = C_D |v^a|^2$, where $U^a = (u_a, v_a)$ is the air velocity and $C_D (= 1, 2.10^{-3})$ a friction coefficient.

We study hereafter four different formulations for the eddy coefficients $\nu_1 = f_1(R)$ and $\nu_2 = f_2(R)$. Functions f_1 and f_2 can be defined as

$$f_1(R) = \alpha_1 + \frac{\beta_1}{(1 + 5R)^2}, \quad f_2(R) = \alpha_2 + \frac{f_1(R)}{1 + 5R} = \alpha_2 + \frac{\alpha_1}{1 + 5R} + \frac{\beta_1}{(1 + 5R)^3}. \quad (3)$$

Formulation (3) corresponds to the modelization of the vertical mixing proposed by Pacanowski and Philander [25]. They proposed for coefficients α_1, β_1 and α_2 the following values: $\alpha_1 = 1.10^{-4}$, $\beta_1 = 1.10^{-2}$, $\alpha_2 = 1.10^{-5}$ (units: $m^2 s^{-1}$). This formulation has been used in the OPA code developed in Paris 6 University [2],[19] with coefficients $\alpha_1 = 1.10^{-6}$, $\beta_1 = 1.10^{-2}$, $\alpha_2 = 1.10^{-7}$ (units: $m^2 s^{-1}$). The selection criterion for the coefficients appearing in these formulas was the best agreement of numerical results with observations carried out in different tropical areas. A variant of formulation (3), proposed by Gent [8], is

$$f_1(R) = \alpha_1 + \frac{\beta_1}{(1+10R)^2}, \quad f_2(R) = \alpha_2 + \frac{\beta_2}{(1+10R)^3} \quad (4)$$

with $\alpha_1 = 1.10^{-4}$, $\beta_1 = 1.10^{-1}$, $\alpha_2 = 1.10^{-5}$, $\beta_2 = 1.10^{-1}$ (units: $m^2 s^{-1}$). A formulation similar to (4) when replacing $10R$ by $5R$ and varying the values of the coefficients α_1, α_2 between the surface and the depth 50m is used in [9].

In this paper, we will also study the properties of two other formulations close to formula (3):

$$f_1(R) = \alpha_1 + \frac{\beta_1}{(1+5R)^2}, \quad f_2(R) = \alpha_2 + \frac{f_1(R)}{(1+5R)^2} = \alpha_2 + \frac{\alpha_1}{(1+5R)^2} + \frac{\beta_1}{(1+5R)^4}, \quad (5)$$

and

$$f_1(R) = \alpha_1 + \frac{\beta_1}{(1+5R)^2}, \quad f_2(R) = \alpha_2 + \frac{\beta_2}{(1+5R)^2}, \quad (6)$$

with $\alpha_1 = 1.10^{-4}$, $\beta_1 = 1.10^{-2}$, $\alpha_2 = 1.10^{-5}$, $\beta_2 = 1.10^{-3}$ (units: $m^2 s^{-1}$).

Eddy viscosity ν_1 defined by (5) or (6) is the same as the coefficient given by Pacanowski and Philander. The definition of the eddy diffusivity coefficient ν_2 differs by the exponent of the term $(1+5R)$. Formula (6) is a simplified version of (5) where β_2 can be considered as a mean value of $\nu_1 = f_1(R)$.

In formulas (3) to (6), the eddy coefficients ν_1 and ν_2 are defined as functions of the Richardson number R through the terms $(1+\gamma R)^n$ appearing at the denominator. Hereafter, these four formulations will be denoted respectively by R213, R23, R224 and R22 where R signifies Richardson number and the integer values are the exponents of $(1+\gamma R)$ in the definitions of ν_1 and ν_2 .

Eddy coefficients defined by relations (3) to (6) present all a singularity for a negative value of the Richardson number $R = -0.2$ or $R = -0.1$. We have plotted in Figure 1a the curves $\nu_1 = f_1(R)$. In formulations (3) or (4) the coefficient of eddy diffusivity ν_2 becomes negative for values of R lower than -0.2 or -0.1 , and therefore the model is no more valid. The curves $\nu_2 = f_2(R)$ obtained with formulations (3) (5) and (6) are plotted in Figure 1b, for $R > -0.2$.

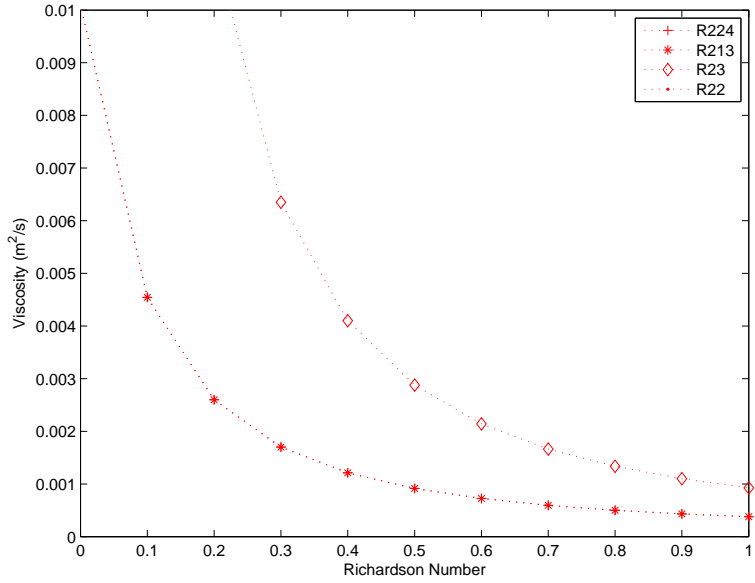


Figure 1a: Viscosity ($\nu_1 = f_1(R)$) for all models

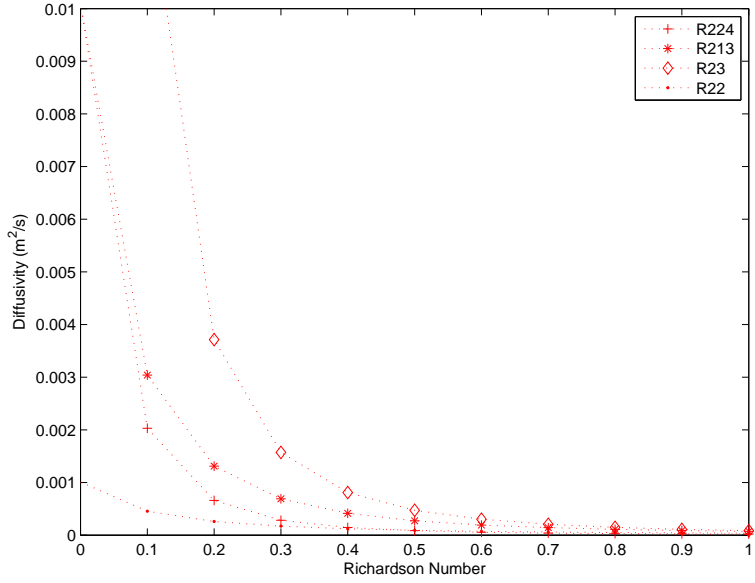


Figure 1b: Diffusivity ($\nu_2 = f_2(R)$) for all models

Problem (2) coupled with one of the definitions (3) to (6) for eddy coefficients retains the vertical shear and buoyancy effect which are two important processes for the generation of the mixed boundary layer, especially in tropical areas.

3 Numerical Experiments

3.1 Finite Difference Scheme

We want to resolve numerically the system (2). We replace the continuous variables $(u, v, \rho, \nu_1, \nu_2)$ by discrete variables $(u_i^n, v_i^n, \rho_i^n, (\nu_1)_i^n, (\nu_2)_i^n)$ which are the approximate solutions at time $n\Delta t$ (with $n = 1, 2, \dots, N$) and at points $(i - NI)\Delta z$ (with $i = 1, 2, \dots, NI$). We discretize the 1D-domain in z-levels where z is the vertical coordinate.

We use a second-order central difference scheme for the second space derivative and a first-order backward difference scheme for the first space derivative. These previous schemes can be written as:

- Second-order central difference scheme: $\left(\frac{\partial^2 u}{\partial z^2}\right)_i^{n+1} = \frac{u_{i+1}^{n+1} - 2u_i^{n+1} + u_{i-1}^{n+1}}{\Delta z^2}$
- First-order backward difference scheme: $\left(\frac{\partial u}{\partial z}\right)_i^{n+1} = \frac{u_i^{n+1} - u_{i-1}^{n+1}}{\Delta z}$

The grid spacing, Δz , is equal to 5 m and the time step, Δt , is equal to 60 s. In time, we use an implicit velocity and implicit density. The viscosity (ν_1) and diffusivity (ν_2) are explicit. The basin depth is 100 m. The boundary conditions are treated with a first-order backward difference scheme. We choose Neumann boundary conditions at the surface and Dirichlet boundary conditions in $z = -h$.

The numerical scheme is the following:

$$\left\{ \begin{array}{l} \frac{u_i^{n+1} - u_i^n}{\Delta t} - \left(\frac{(\nu_1)_i^n - \nu_1)_{i-1}^n}{\Delta z} \right) \cdot \left(\frac{u_i^{n+1} - u_{i-1}^{n+1}}{\Delta z} \right) - \nu_1)_i^n \cdot \left(\frac{u_{i+1}^{n+1} - 2u_i^{n+1} + u_{i-1}^{n+1}}{\Delta z^2} \right) = 0, \\ \frac{v_i^{n+1} - v_i^n}{\Delta t} - \left(\frac{(\nu_1)_i^n - \nu_1)_{i-1}^n}{\Delta z} \right) \cdot \left(\frac{v_i^{n+1} - v_{i-1}^{n+1}}{\Delta z} \right) - \nu_1)_i^n \cdot \left(\frac{v_{i+1}^{n+1} - 2v_i^{n+1} + v_{i-1}^{n+1}}{\Delta z^2} \right) = 0, \\ \frac{\rho_i^{n+1} - \rho_i^n}{\Delta t} - \left(\frac{(\nu_2)_i^n - \nu_2)_{i-1}^n}{\Delta z} \right) \cdot \left(\frac{\rho_i^{n+1} - \rho_{i-1}^{n+1}}{\Delta z} \right) - \nu_2)_i^n \cdot \left(\frac{\rho_{i+1}^{n+1} - 2\rho_i^{n+1} + \rho_{i-1}^{n+1}}{\Delta z^2} \right) = 0. \end{array} \right. \quad (7)$$

The residual are computed as:

$$r^n = \left(\sum_{i=1}^{NI} |u_i^{n+1} - u_i^n|^2 + \sum_{i=1}^{NI} |v_i^{n+1} - v_i^n|^2 + \sum_{i=1}^{NI} |\rho_i^{n+1} - \rho_i^n|^2 \right)^{1/2}. \quad (8)$$

3.2 Linear case

In this section, the initial profiles are linear as Tabak and al [29] and Deleersnijder [5]. We compare the four turbulence model. We use three criteria: the surface current intensity, the thermocline's form and the mixed layer depth. We study two case: a low surface wind and a strong surface wind. These different cases aim to validate our code thanks the model sensitivity to the wind stress(mixed layer formation, surface current intensity ...). Furthermore, we seek for the four models behavior in this particular case. In each experiment, the buoyancy flux is equal to $-1.10^{-6} \text{ kg.s}^{-1}.\text{m}^{-2}$. It corresponds to the static stability case. The model is integrated for 48 hours.

3.2.1 First case: Low surface wind

In this first simulation, the zonal wind at the surface is equal to 3 m.s^{-1} (eastward wind) and the meridional wind is equal to 0.4 m.s^{-1} (northward wind). The initial density profile (see figure 2) does not display a mixed layer. Notice that the initial linear profiles are not realistic.

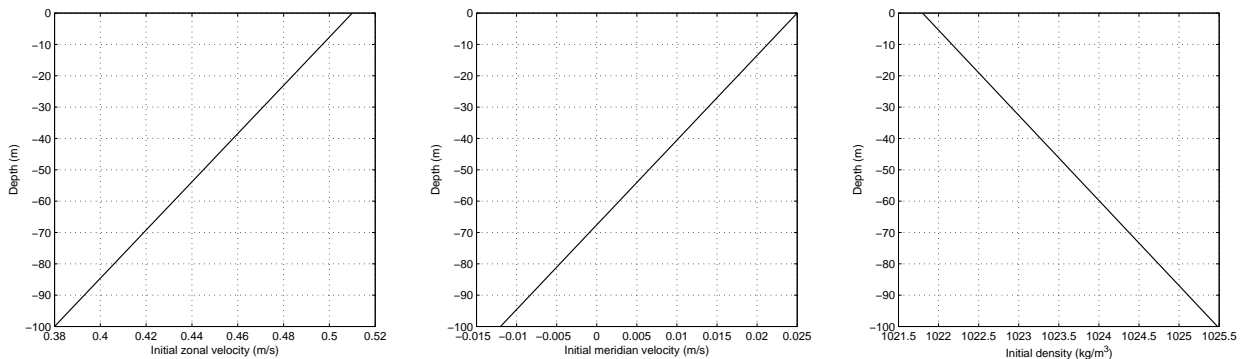


Figure 2: Initial zonal velocity, meridian velocity and density profile (left to right).

The results of the numerical simulations are displayed on figure 3. We compare the different parametrization of the vertical mixing by means of zonal velocity profile (left position), meridian velocity profile (medium position) and density profile (right position). The entire water column is displayed on the bottom row. We have plotted the surface flow on the top row. The residual are displayed on figure 4. On figure 3 and 4, the R224 model is marked by an asterisk, the R213 model by an plus, the R23 model by a diamond and the R23 model by a triangle.

- We observe a five meters deep mixed layer in case of R213 and R22 models. R224 and R23 model do not produce a mixed layer.
- The R213 and R23 models yield the same surface current intensity. The R22 model underestimates this current while the R224 model overestimates it in comparison with R213 and R23 models.
- Since, we have applied an eastward wind at the surface, the final zonal surface current intensity is stronger than the initial one. In the same order, since we have applied a

northward wind, the final meridian surface current intensity is stronger than the meridian surface current. However, since the applied meridian wind is low, the differences between the initial configuration are small.

- Since, we have applied a low surface wind, the deep flow is the same as the initial time. The surface fluxes are not enough strong to modify the deep flow.

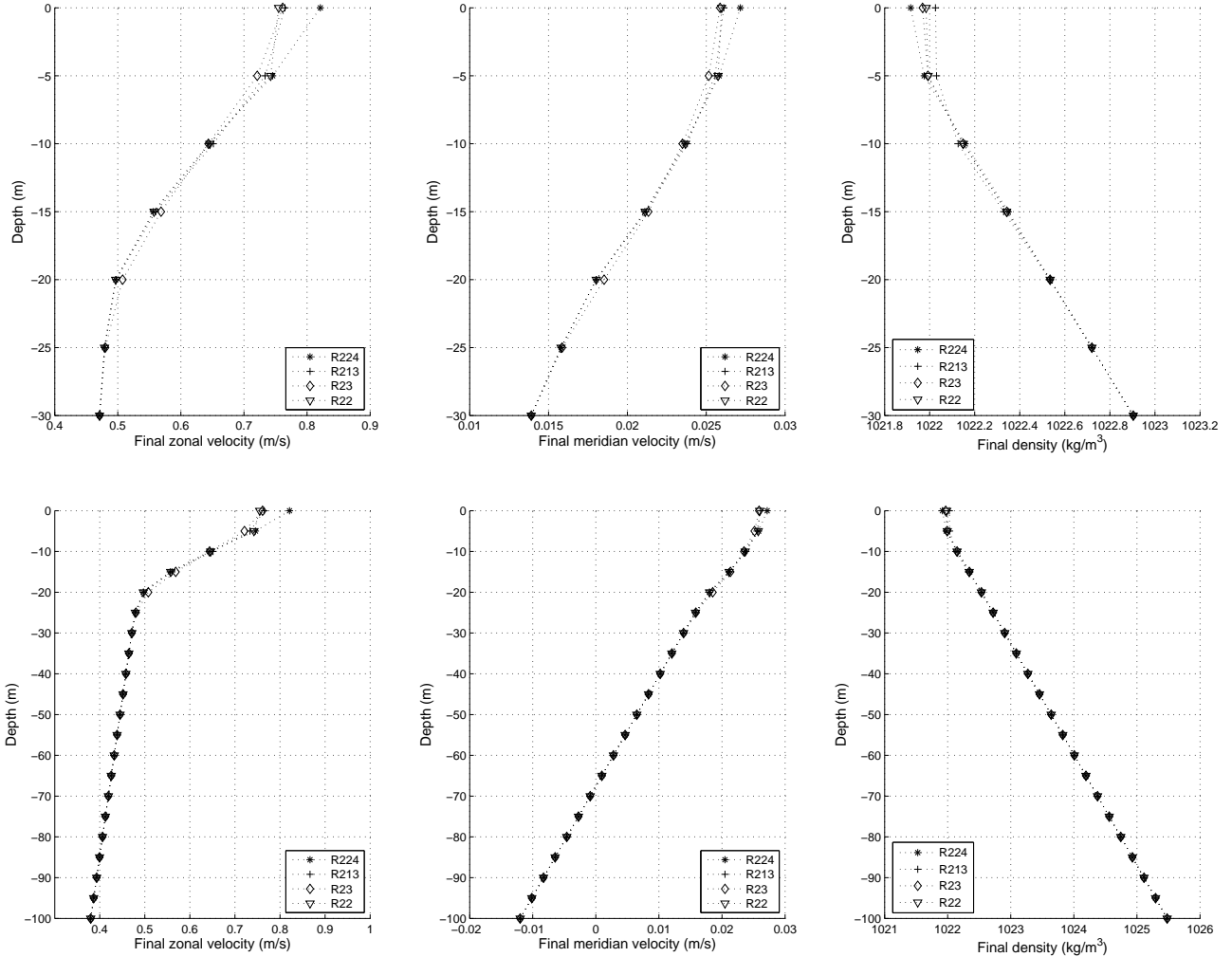


Figure 3: Comparison of zonal velocity profiles (left position), meridional velocity profiles (medium position) and density profiles (right position).

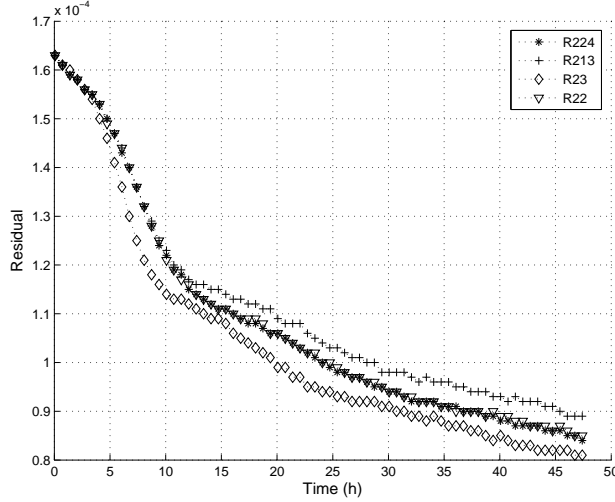


Figure 4: Comparison of residual values.

The residual are computed thanks the expression 8 and decrease gradually in the time for all models. Hence, the numerical convergence is good.

3.2.2 Second case: Strong surface wind

We now study the case of a strong surface wind. The model is still integrated for 48 hours. At the surface, the zonal wind is equal to 11.7 m.s^{-1} (eastward wind) and a meridional wind is equal to 0.4 m.s^{-1} (northward wind). We keep a surface buoyancy flux equal to $1.10^{-6} \text{ kg.s}^{-1} \text{ m}^{-2}$. The results are displayed on figure 5.

- The formation of a mixed layer is observed in case of R23, R224 and R213 model according to the same criterion as Peter and al [27]. This mixed layer is ten meters deep. R22 model product a five meters deep mixed layer as in the low wind case.
- The R213 and R224 models give same results for the surface current intensity. The R23 model underestimates this current while R22 overestimates it in comparison with R213 and R224 models.
- As the bottom of the mixed layer corresponds either to the top of the thermocline, the thermocline simulated by R213, R23 and R224 models are similar.
- The results obtained with the four models are not very different in the lower layer (60-100m) because the surface fluxes do not affect the deep water column.

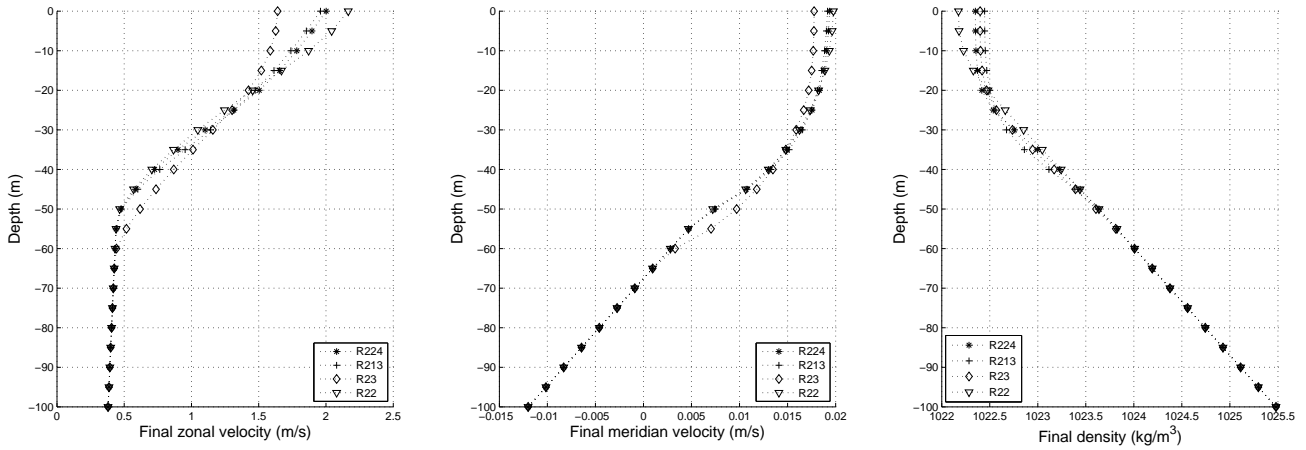


Figure 5: Comparison of zonal velocity profiles (left position), meridional velocity profiles (medium position) and density profiles (right position).

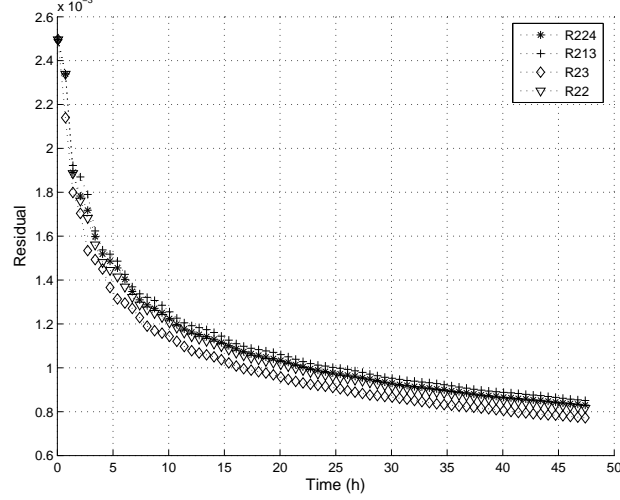


Figure 6: Comparison of residual values.

On figure 6, the residual time evolution (decreasing in time) shows a good numerical convergence.

Remark:

The final diffusivity and viscosity are displayed on figure 7 in case of all models. We observe the order described below.

$$(\nu_1)_{23} > (\nu_1)_{213} \simeq (\nu_1)_{224} > (\nu_1)_{22}$$

$$(\nu_2)_{23} > (\nu_2)_{213} \simeq (\nu_2)_{224} > (\nu_2)_{22}$$

The R23 model has a strongest viscosity and diffusivity. Therefore, the R23 surface current is lower than the others surface current. In the same order, the R22 model has a lowest viscosity

and diffusivity and hence, the R22 surface current is stronger than the others surface current. As the R224 viscosity and diffusivity are similar, the R224 and R213 surface current are similar. However, the R224 surface current is slightly stronger than the R213 surface current.

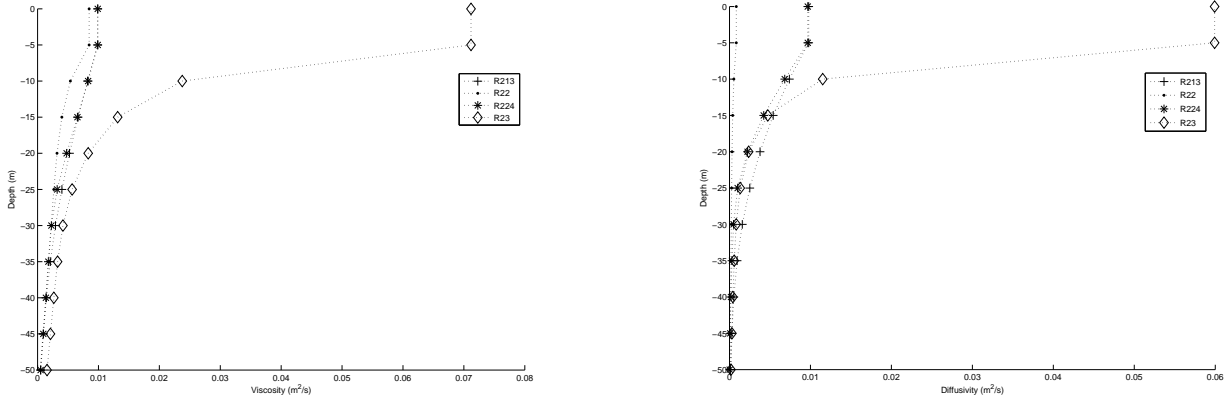


Figure 7: Final viscosity and final diffusivity (from left to right) in case of all models.

3.2.3 Summary of the linear case

- We observe, for all models, sensitivities to the wind stress intensity. When we apply a northward wind ($v > 0$) at the surface, the meridional surface current values increase in comparison with the initial values. In the same order, a eastward wind ($u > 0$) at the surface yields an increasing in the zonal surface current values. This fact is in agreement with the physical reality. Two of four models, R22 and R213, produce a mixed layer in a low wind case. We observe, for the strong wind case, the formation of a mixed layer for all models. This formation is in agreement with observations because a strong wind increase the mixing. Furthermore, the residual decrease in time for all models in case of a strong surface wind and a low surface wind. Our code yields realistic results and the numerical convergence is good. All these previous remark valid our code.
- The surface current simulated by R224 model is similar to the R213 surface current in the linear strong wind case and it is similar to the R23 surface current in the linear low wind case. R22 model overestimates this current in strong surface wind case. In the linear strong wind case, R224, R213 and R23 models yields the same mixed layer depth and the same thermocline. However, R22 model simulates a shallower mixed layer. Since R213 and R23 model are known to give realistic results, the R224 model is good for the mixed layer simulation. The R22 results are not satisfactory.

3.3 Realistic case

In this section, we aims to study a equatorial Pacific region called the West-Pacific Warm Pool. So, we initialize the code with data from the TAO array (McPhaden [20]). It is located at the

equator between $120^{\circ}E$ and $180^{\circ}E$. The sea temperature is high and quasi-constant along the year ($28 - 30^{\circ}C$). The precipitation are intense and hence the salinity is low. In the first part, we study a long time case. We investigate, in the second part, the behavior of four turbulence models in case of low surface wind and strong surface wind. In the last part, we seek for the behavior of four models in case of an particular initial density profile. This profile presents a static instability zone located between -30 m and -50 m .

3.3.1 The initial data

We use data available from the Tropical Atmosphere Ocean (TAO) array (McPhaden [20]). The TAO project aims to study the exchange between the tropical oceans and the atmosphere. The TAO data have been very used in numerical simulations. The velocity data comes from the ACDP (Acoustic Doppler Current Profiler) measurements. To obtain the appropriate profiles, we interpolate the data by an one-order linear interpolation. We initialize our code with these profiles and we obtain the results below.

3.3.2 Numerical Results

Equilibrium solution We simulate a long time case. This study aims to confirm the results of Bennis and al ([1]). In this paper, the authors have been shown that the final profiles became linear in long time. So, the model is integrated for 10000 hours. However, the profiles are already linear for an integrated time of 2500 hours. The initial profiles represent the ocean mean state in June 17, 1991. The buoyancy flux is equal to $-1.10^{-6}\text{ kg.m}^{-2}.s^{-1}$ corresponding to heat flux equal, in absolute value, to 11 W/m^2 . This heat flux is in agreement with Gent [8]. The heat flux, between $140^{\circ}E - 180^{\circ}E$ and $10^{\circ}N - 10^{\circ}S$, is in the range $[0\text{ W/m}^2 ; 20\text{ W/m}^2]$. In the next, we will apply the same heat flux. The surface zonal wind is equal to 5.4 m.s^{-1} (eastward wind) and the surface meridional wind is equal to 0.9 m.s^{-1} (northward wind). The initial profiles are displayed on figure 8.

- Initial zonal velocity profile: We observe two eastward currents located at the surface and around to -70 m . There are two westward currents located around to -45 m and -90 m .
- Initial meridian velocity profile: There are several southward current and northward current. The main southward current is located around to -55 m . The main northward current are located around to -90 m and at the surface.
- Initial density profile: There is a thirty five meters deep mixed layer according to Peters and al's [27] criterion.

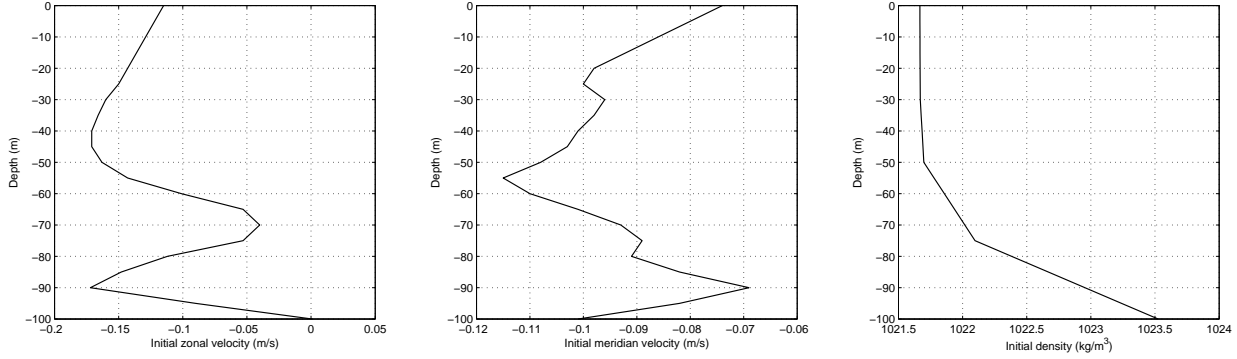


Figure 8: The initial profile of zonal velocity, meridional velocity, in-situ density (left to right).

The numerical results are displayed on figure 9. The R224 results are marked by an asterisk, the R213 results by a plus, the R23 results by a diamond and the R22 results by a triangle. The four turbulence models give a linear profile for the simulated time. This fact corroborates the existence of a linear equilibrium solution obtained by Bennis and al [1]. The R213, R224 and R23 models give similar density profiles. The velocity simulated by R213 and R224 models are similar. The R23 zonal and meridional velocity are lower than the others. The R22 zonal and meridional velocity are stronger than the others.

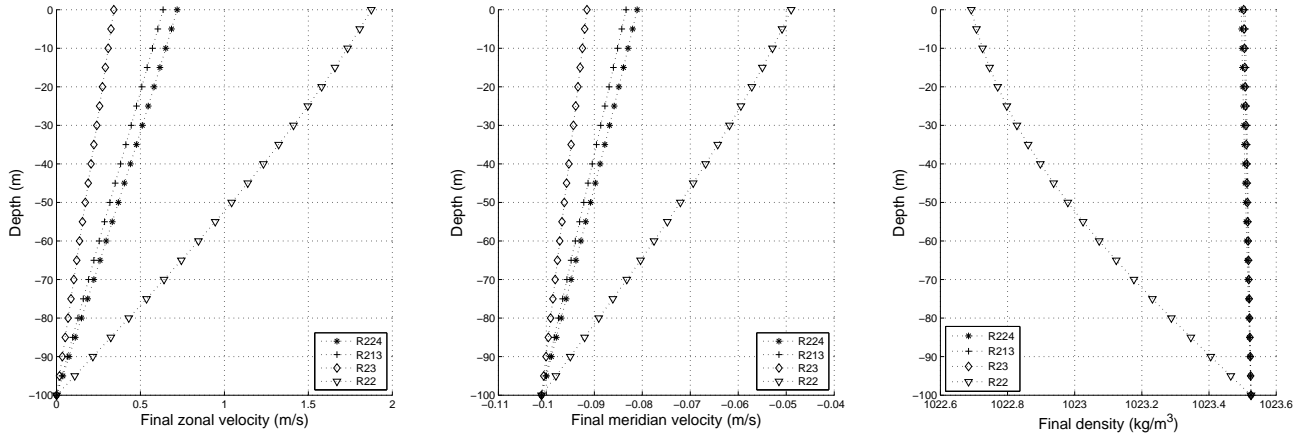


Figure 9: Comparison of zonal velocity profiles (left position), meridional velocity profiles (medium position) and density profiles (right position).

The residual are displayed on figure 10. Notice that the numerical convergence is good for all models.

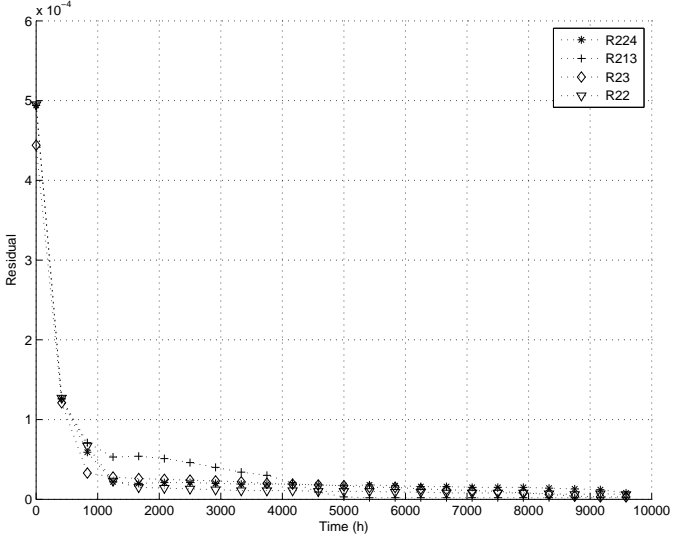


Figure 10: Comparison of residual values.

Sensitivity to the wind stress We investigate this sensitivity with initial realistic data for the time period between the June 15, 1991 and July 15, 1991. The initial profiles are displayed on figure 11. The initial zonal velocity profile presents a westward current at the surface and, below it, an eastward undercurrent whose maximum is located about 55 m. Deepest, we observe a westward undercurrent. The initial density profile does not display a mixed layer.

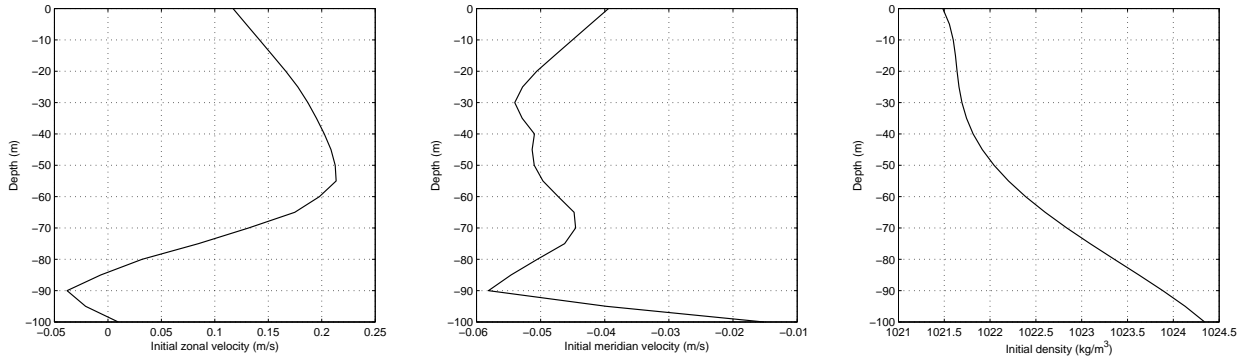


Figure 11: Initial zonal velocity, meridian velocity and density profiles

The buoyancy flux is equal to $-1.10^{-6} \text{ kg.m}^{-2}.\text{s}^{-1}$. The model is integrated for 48 hours. We start by studying a low surface wind. The zonal wind is equal to 2.1 m/s (eastward wind) and a meridional wind is equal to 1.0 m/s (northward wind). The second case is less realistic than the first case. The wind stress is stronger than in reality. These values correspond to an another period in the studied year. The zonal wind is equal to 8.1 m/s (eastward wind) and the meridional wind is equal to 2.1 m/s (northward wind).

The numerical results are displayed on figures 13 and 15. In the low wind case, the surface current computed by R23 and R224 models are similar. The R22 and R213 surface current are lower than the others surface currents. The final density profile does not display a mixed layer for all models. Therefore, we cannot study the mixed layer depth nor the thermocline's form. In the strong wind case, the R213 and R224 surface current values are similar. The R23 model surface current is lower than the R213 and R224 surface current. The R22 surface current is stronger than the R213 and R224 surface current. The final density profile display a twenty meters deep mixed layer for R213, R224, R23 models. The R22 model products a five meters deep mixed layer. Furthermore, the thermocline computed by R224, R213 and R23 models are similar. The deep flow ($60 - 100\text{ m}$) are similar for all models because the surface fluxes are not enough strong to affect the deep water.

The surface current behavior can be explain by the viscosity and diffusivity values. In case of strong surface wind, the final diffusivity and viscosity are displayed on figure 12 for all models. We observe the order described below.

$$\begin{aligned} (\nu_1)_{23} &> (\nu_1)_{213} \simeq (\nu_1)_{224} > (\nu_1)_{22} \\ (\nu_2)_{23} &> (\nu_2)_{213} \simeq (\nu_2)_{224} > (\nu_2)_{22} \end{aligned}$$

The R23 model has a strongest viscosity and diffusivity. Therefore, the R23 surface current is lower than the others surface current. In the same order, the R22 model has a lowest viscosity and diffusivity and hence, the R22 surface current is stronger than the others surface current. As the R224 viscosity and diffusivity are similar, the R224 and R213 surface current are similar. However, the R224 surface current is slightly stronger than the R213 surface current.

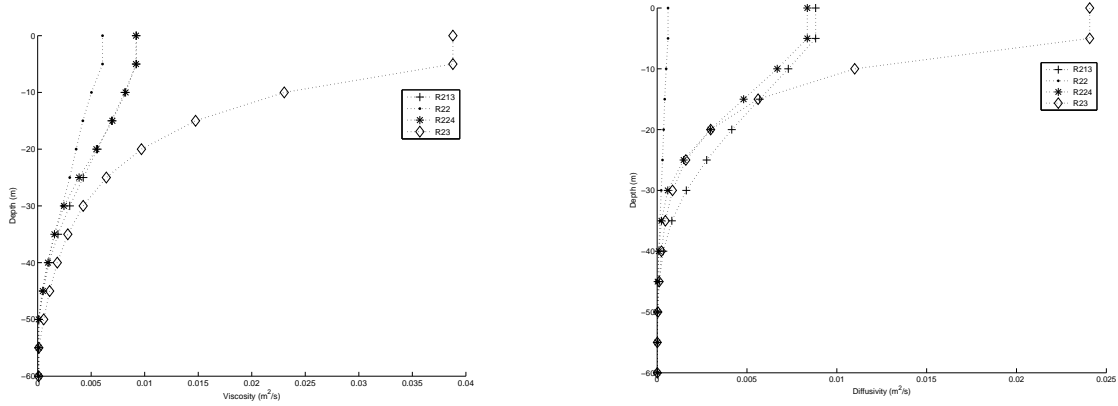


Figure 12: Final viscosity (left hand side) and final diffusivity (right hand side) for all models.

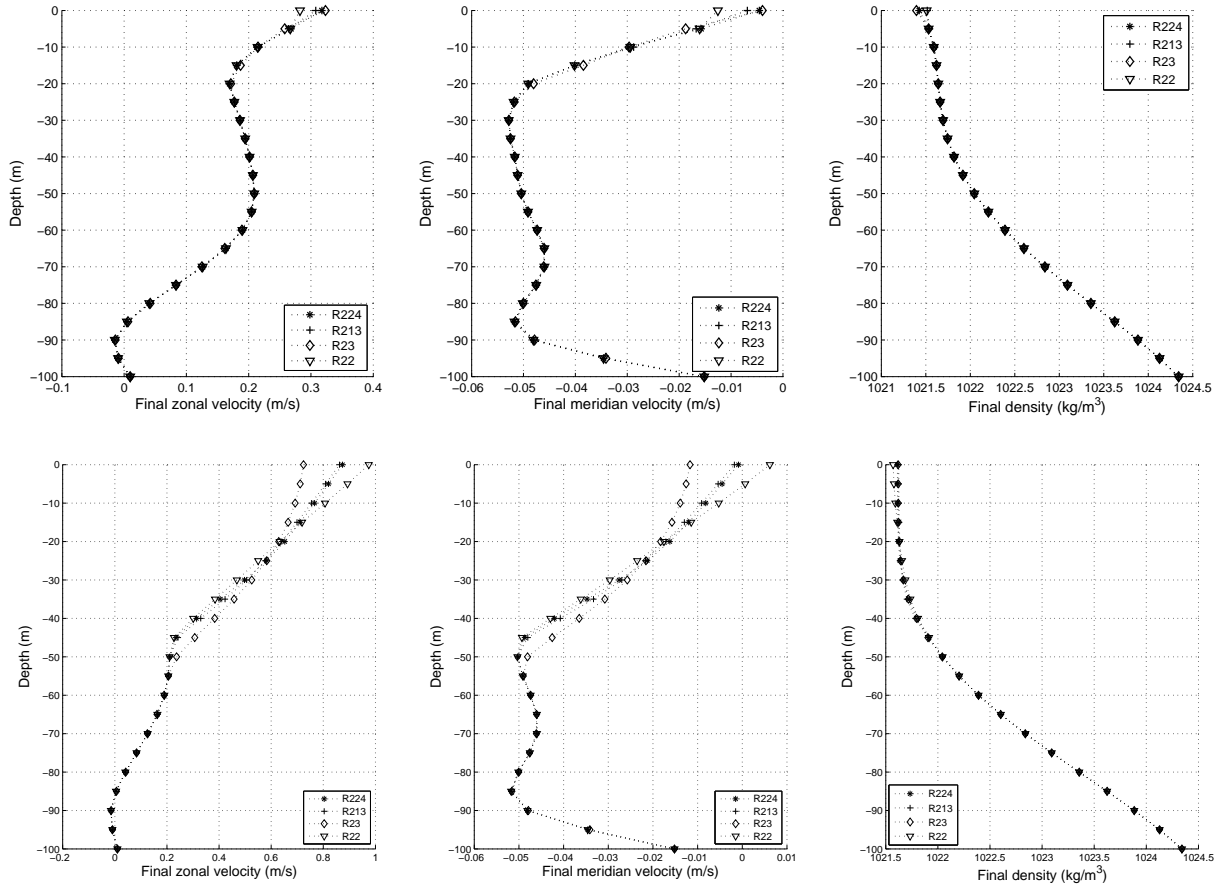


Figure 13: Comparison of four turbulence model in the low wind case (top row) and in the strong wind case (bottom row).

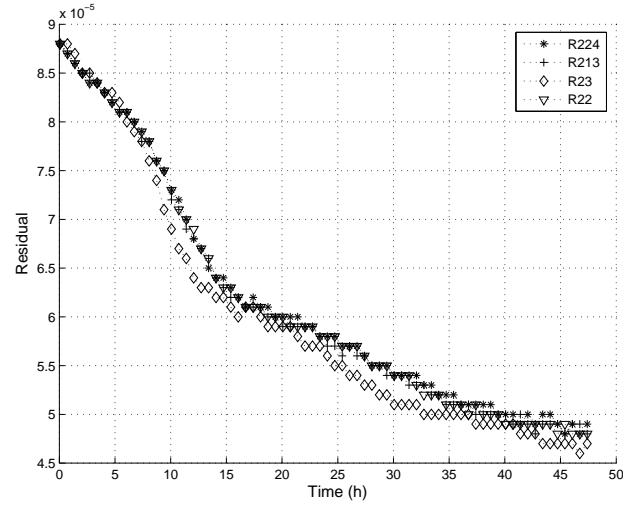


Figure 14: Comparison of residual values in case of low surface wind.

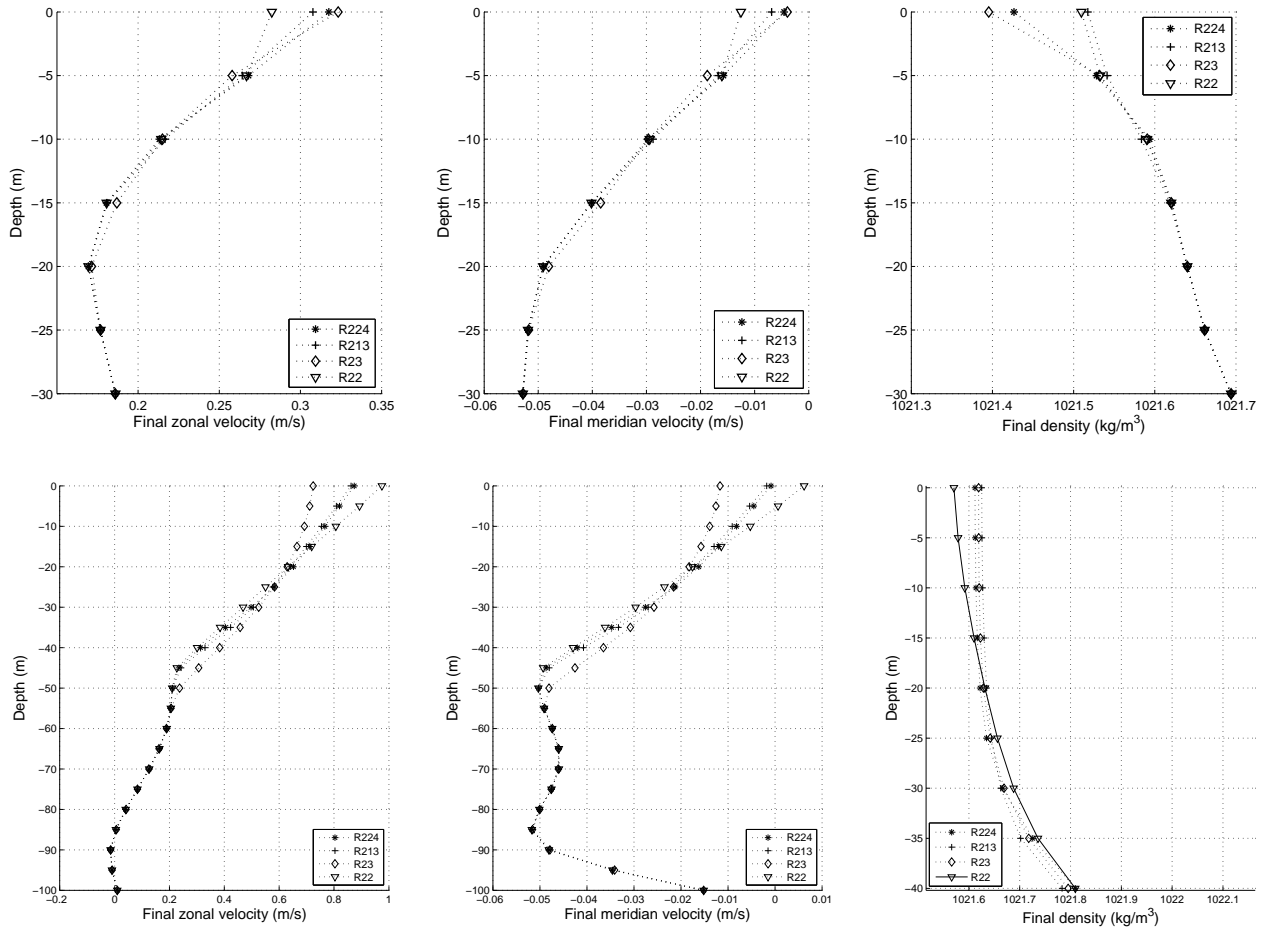


Figure 15: Zoom on shallow flow. Comparison of four turbulence model in the low wind case (top row) and in the strong wind case (bottom row).

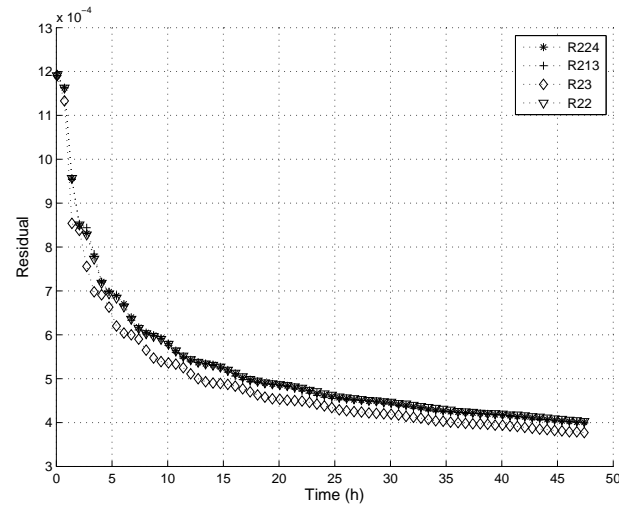


Figure 16: Comparison of residual values in case of strong surface wind.

On figure 14 and 16, we observe a good numerical convergence in case of low surface wind and in case of strong surface wind. Furthermore, it is right for all models.

Sensitivity to the initial density flux The code is initialized with 17 November 1991 data's. The initial zonal velocity profile displays a eastward current whose maximum is located about 55 m. The initial meridian velocity profile displays a southward current whose maximum is located about 20 m. The initial density profile displays a static instability zone between -30 m and -50 m . Notice that there is a seventy meters deep mixed layer. However, this mixed layer is not homogeneous. The initial profiles are displayed on figure 17.

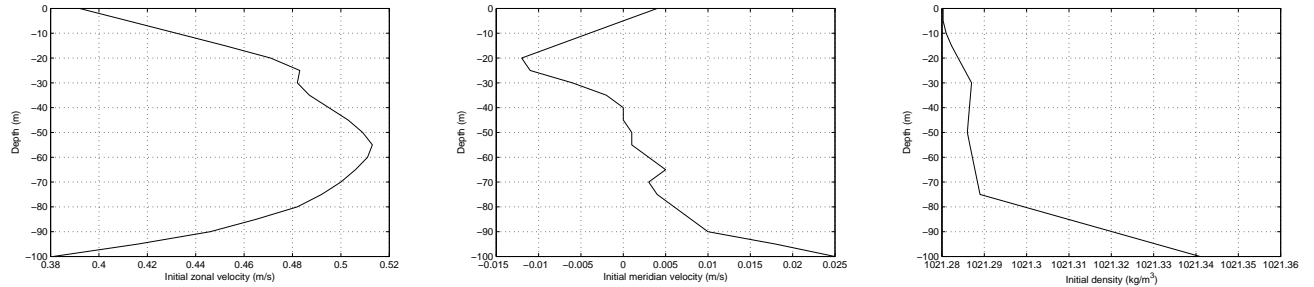


Figure 17: The initial profile for zonal velocity, meridian velocity and density for the different depths.

On figure 18, the initial richardson number, called R^0 , is near to -0.2 for $z = -45\text{ m}$. The R22, R213 and R224 models have infinite viscosity and diffusivity for $R^0 = -0.2$. Hence, the R213 diffusivity (see figure 20) and the R224, R22 diffusivity (see figure 19) are large for this depth. The initial richardson number (see figure 18) is inferior to -0.2 for $z = -35\text{ m}$ and $z = -50\text{ m}$. Therefore, the R213 diffusivity is negative. In the range $[-35\text{ m}, -50\text{ m}]$, the initial richardson number is inferior to -0.1 and hence the R23 diffusivity is negative. On figure 20, the negative diffusivity is marked by a point for R23 and R213 models. On figure 21, the negative diffusivity is marked by an asterisk for R213 model. The R22 and R224 diffusivity (see figure 19) are not negative. In physical reality, there are not negative diffusivity. The diffusivity was estimated by Osborn and Cox [24] with measurements of very small scale vertical structure. In our studied region, the diffusivity is in the range $[1.10^{-2}\text{ cm}^2.\text{s}^{-1}, 1.10^3\text{ cm}^2.\text{s}^{-1}]$. Notice that the diffusivity is always positive. So, we can not use R213 and R23 models for this case.

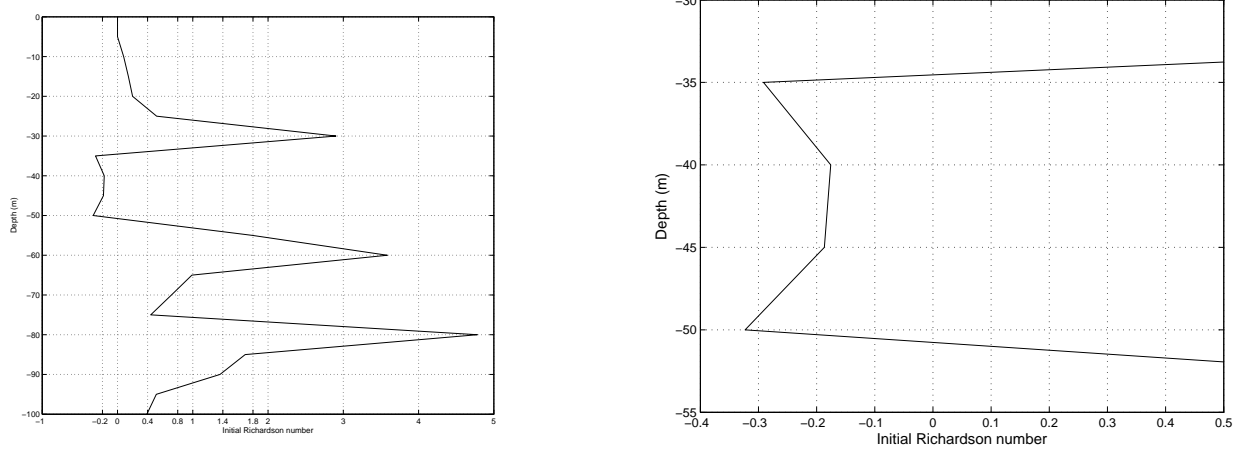


Figure 18: The initial richardson number for the different depths.

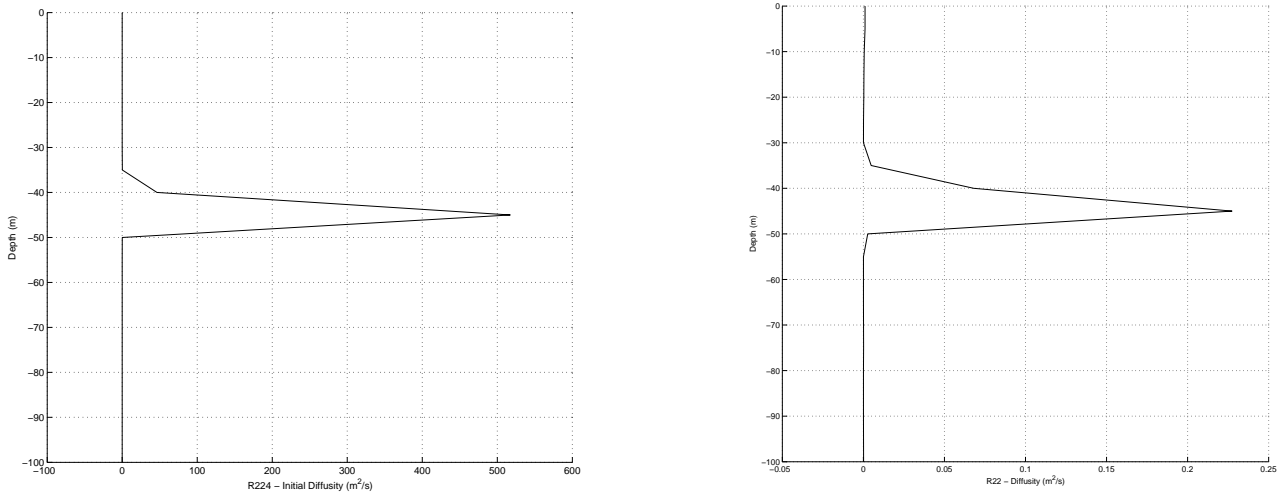


Figure 19: Initial diffusivity for formulations R224 (left hand side) and R22 (right hand side).

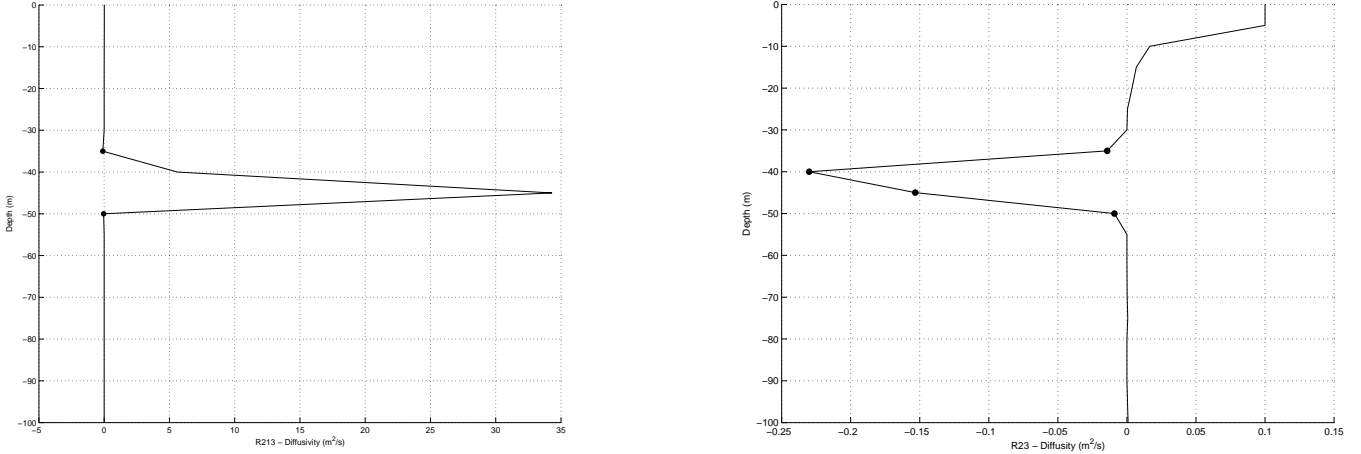


Figure 20: Initial diffusivity for formulations R213 (left hand side) and R23 (right hand side).

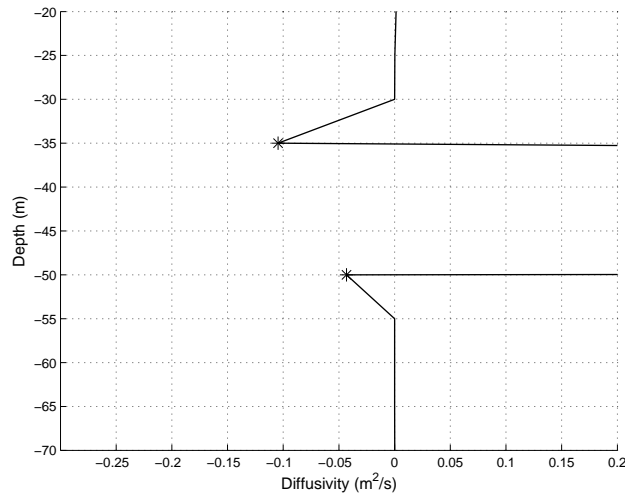


Figure 21: Zoom on the R213 negatives values marked by an asterisk.

The model is integrated for 48 hours. The zonal wind is equal to 11.7 m.s^{-1} (eastward wind). The meridional wind is equal to 0.4 m.s^{-1} (northward wind). The buoyancy flux is equal to $-1.10^{-6} \text{ kg.m}^{-2}.\text{s}^{-1}$. The results are displayed on figure 22. The R22 model does not produce a mixed layer. The R224 model produces an homogeneous seventy meters deep mixed layer. This layer is homogeneous because we have applied a negative buoyancy flux. This flux stabilizes the flow. The R22 surface current is stronger than the R224 surface current. This fact is in agreement with the previous results. The R22 and R224 models give similar results into the range $[-100 \text{ m}, -60 \text{ m}]$. The surface fluxes do not affect the deep water.

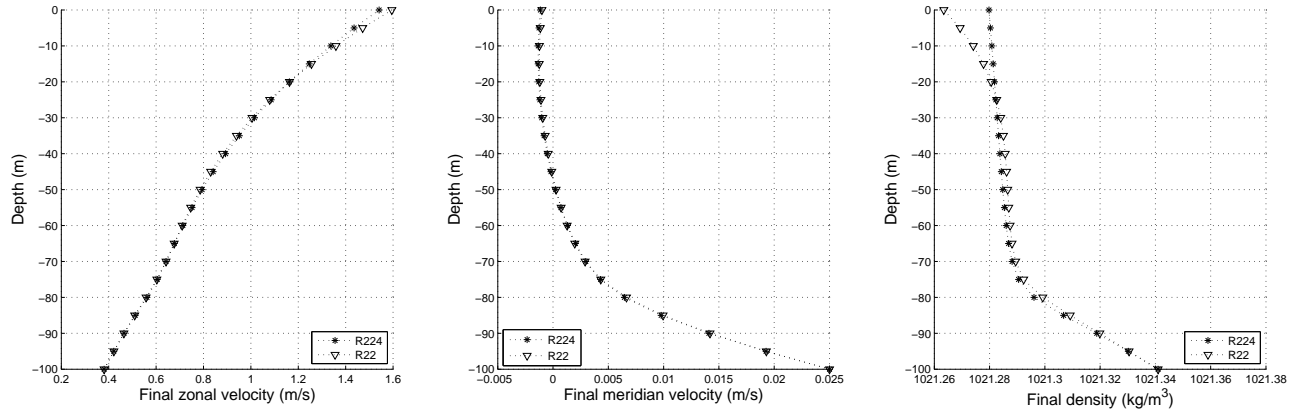


Figure 22: Comparison of zonal velocity profiles (left position), meridional velocity profiles (medium position) and density profiles (right position).

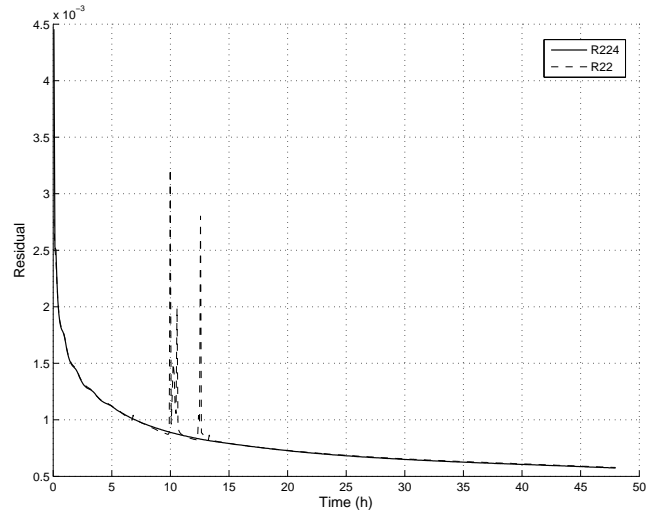


Figure 23: Comparison of residual values.

The residual values show a good numerical convergence for R224 models (solid line). The R22 model (dotted line) presents three divergence points for 10 hours, 11 hours and 13 hours. However, the R22 numerical convergence is good.

Summary of the realistic case

- The R23 and R224 surface current are similar in case of a low surface wind. R22 and R213 surface current are lower than the R23 and R224 surface current. In the realistic strong wind case, the R224 and R213 surface current are similar. The R23 surface current is weaker than the R224 and R213 surface current. On the contrary, the R22 surface current is stronger.

- The formation of a mixed layer is observed for all models in the strong wind case. The mixed layer depth and the thermocline's form are the same in case R213, R23, R224 models.
- The R213 and R23 model are not physically valid in the case of static instability where $R < -0.2$. R22 and R224 models are valid and only R224 model gives good results.

4 Summary and Discussion

4.1 Code validation

The sensitivity to the wind stress (a mixed layer formation, an increase/decrease in surface current) are similar in linear case and in realistic case. We explain this below:

- In the strong wind case, we observe the formation of a mixed layer when the wind increases. It is a physical phenomenon. The more strong the wind is, the more intense the mixing is. Hence the mixed layer depth increases.
- When we apply an eastward wind ($u > 0$) at the surface, we observe an increase in the zonal surface current. In the same order, a northward wind ($v > 0$) at the surface causes an increase in the meridional surface current. These results are in agreement with the physical reality.
- The more strong the surfaces fluxes are, the more affected the deep flow is. It is physically right.

Furthermore, the residual are good in all cases. Theses previous remarks valid our code. It gives a good representation of the physical reality.

4.2 Comparison of four turbulence models

Our comparison is based on three criterion: the mixed layer depth, the surface current intensity and the thermocline's form. The mixed layer depth is obtained with a density difference criterion. This difference is equal to 0.01 kg.m^{-3} . We use the surface current values to determine the surface current intensity. The density gradient is used to determine the thermocline's form. We summarize the results hereafter.

- The R213, R23 and R224 model give a same mixed layer depth. The R22 model product a shallowest mixed layer. The R224 mixed layer depth is lower than the R213, R23 mixed layer depth in the long time case. The formation of mixed layer depends on the wind stress intensity.
- The R224 and R213 surface current are similar for the linear and realistic strong wind case. However the R224 surface current is slightly stronger than the R213 surface current. R23 model underestimate this current while the R22 model overestimate it.

- The R23 and R224 model surface current are similar for the realistic low wind case. The R213 surface current is slightly weaker than the R23 and R224 surface current. In the linear low wind case, the R213 and R23 surface current are the same. The R224 surface current is stronger than the R213 and R23 surface current. The R22 surface current is not good in the two cases.
- The R224 and R213 surface current are the same behavior in the long time. The R23 model underestimate this current whereas R22 model overestimate it. The long time profiles are linear. It is in agreement with Bennis and al [1].
- The R23, R213 and R224 thermocline are similar in the linear and realistic strong wind case.
- In case of static instability, the R213 and R23 models are a negative diffusivity at the initial time. Therefore, these model are not physically valid in this case. This problem comes from to the reverse density gradient around to -30 m . Hence, we can not use these model in this case. Only, R224 and R22 models are valid. The R22 model does not products a mixed layer. R224 model product an homogeneous mixed layer without increase its depth. R224 surface current is weaker than the R22 surface current.

Finally, we conclude that the R22 model is not accurate to simulate a mixed layer as well as the surface current. The R224 and R213 surface current are similar in realistic and linear strong wind case. In the realistic low wind case, the R224 surface current is similar to the R23 surface current. The R23 and R213 model are known for doing a realistic mixed layer. Therefore, the R224 model is good for the surface current simulation in the previous cited case. However, in the low wind case, the R224 model is inferior to the others models. The R224 thermocline is similar to the R23 and R213 thermocline. Hence, the R224 is also good for thermocline simulations. In case of static instability, only R224 model is physically valid and it gives a homogeneous mixed layer.

On the whole, the R224 model has the same behavior as the Pacanowski and Philander model (R213 model) and we can use it in more situation.

References

- [1] A. C. BENNIS, T. C. REBOLLO, M. G. MARMOL, AND R. LEWANDOWSKI, *Stability of some turbulent vertical models for the ocean mixing boundary layer*, Applied Mathematical Letters, To Appear (2007).
- [2] B. BLANKE AND P. DELECLUSE, *Variability of the tropical atlantic ocean simulated by a general circulation model with two different mixed-layer physics*, J. Phys. Oceanography, 23 (1993), pp. 1363–1388.

- [3] K. BRAINERD AND M. GREGG, *Surface mixed layer and mixing layer depths*, Deep Sea research, 42 (1995), pp. 1521–1543.
- [4] J. W. DEARDORFF, G. WILLIS, AND D. LILLY, *Laboratory investigation of nonsteady penetrative convection*, J. Fluid. Mech., 35 (1969), pp. 7–31.
- [5] E. DELEERSNIJDER, *Echelles de temps déterminant, ou déterminées par, les écoulements des fluides géophysiques*, Bul. Soc. Roy. Sci. Liège, 67 (1998), pp. 43–68.
- [6] A. GARGETT AND T. R. OSBORN, *Small scale shear measurements during the fine and microstructure experiment*, J. Geophys. Res., 86 (1981), pp. 1929–1944.
- [7] P. GASPAR, Y. GREGORIS, AND L. J. M., *A simple eddy kinetic energy model for simulations of the oceanic vertical mixing: test at station papa and long-term upper ocean study site*, J. Geophys. Research, 16 (1990), pp. 179–193.
- [8] P. R. GENT, *The heat budget of the toga-coare domain in an ocean model*, J. Geophys. Res., 96 (1991), pp. 3323–3330.
- [9] H. GOOSSE, E. DELEERSNIJDER, T. FICHEFET, AND M. H. ENGLAND, *Sensitivity of a global coupled ocean-sea ice model to the parametrization of vertical mixing*, J. Geophys. Res., 104 (1999), pp. 13681–13695.
- [10] M. C. GREGG, *Temperature and salinity microstructure in the pacific equatorial undercurrent*, J. Geophys. Res., 81 (1976), pp. 1180–1196.
- [11] M. C. GREGG AND T. B. SANDFORD, *Signature of mixing from the bermuda slope, the sargasso sea and the gulf stream*, J. Phys. Oceanogr., 10 (1980), pp. 105–127.
- [12] D. HALPERN, Y. CHAO, C. MA, AND C. MECHOSO, *Comparison of tropical pacific temperature and current simulations with two vertical mixing schemes embedded in ocean general circulation model and reference to observations*, J. Geophys. Res., 100 (1995), pp. 2515–2523.
- [13] A. C. HIRST AND T. J. M. DOUGALL, *Deep-water properties and surface buoyancy flux as simulated by a z-coordinate model including eddy-induced advection*, J. Phys. Oceanogr., 26 (1996), pp. 1320–1343.
- [14] R. H. KÄSE, *Modeling of the oceanic mixed-layer and effects of deep convection*, 1998.
- [15] E. KRAUS AND J. TURNER, *A one dimensional model of the seasonal thermocline, ii, the general theory and its consequences*, Tellus, 19 (1967), pp. 99–105.
- [16] W. G. LARGE, C. McWILLIAMS, AND S. C. DONEY, *Oceanic vertical mixing : a review and a model with a nonlocal boundary layer parametrization*, Rev. Geophys., 32 (1994), pp. 363–403.
- [17] M. LESIEUR, *Turbulence in Fluids*, Kluwer, 1997.

[18] X. LI, Y. CHAO, J. MCWILLIAMS, AND L. FU, *A comparison of two vertical-mixing schemes in a pacific ocean general circulation model*, Journal of Climate, 14 (2001), pp. 1377–1398.

[19] G. MADEC, P. DELECLUSE, M. IMBARD, AND C. LEVY, *O.p.a. version 8.0. ocean general circulation model, reference manual*, 1997. Technical report.

[20] M. MCPHADEN, *The tropical atmosphere ocean (tao) array is completed*, Bull. Am. Meteorol. Soc, 76 (1995), pp. 739–741.

[21] G. MELLOR AND T. YAMADA, *Development of a turbulence closure model for geophysical fluid problems*, Reviews of Geophysics and Space Physics, 20 (1982), pp. 851–875.

[22] C. B. MONTEGUT, G. MADEC, A. S. FISCHER, A. LAZAR, AND D. IUDICONE, *Mixed layer depth over the global ocean : An examination of profile data and a profile-based climatology*, Journal Geophysical Research, 109 (2004), p. C12003.

[23] P. P. NIILER AND COAUTHORS, *Comparison of toga tropical pacific ocean model simulations with the woce/toga surface velocity programme drifter data set.*, World Climate Research Programme Rep. WCRP-1995, (1995), p. 156pp.

[24] T. OSBORN AND C. COX, *Oceanic finestructure*, Geophys. Fluid Dyn., 3 (1972), pp. 321–345.

[25] R. C. PACANOWSKI AND S. G. H. PHILANDER, *Parametrization of vertical mixing in numericals models of the tropical oceans*, J. Phys. Oceanogr., 11 (1981), pp. 1443–1451.

[26] H. PETERS, M. C. GREGG, AND J. M. TOOLE, *On the parametrization of equatorial turbulence*, Journal of Geophysical Research, 93 (1988), pp. 1199–1211.

[27] ——, *Meridional variability of turbulence through the equatorial undercurrent*, Journal of Geophysical Research, 94 (1989), pp. 18,003–18,009.

[28] S. G. H. PHILANDER, *La Niña, and the Southern Oscillation*, Academic Press, 1990.

[29] E. G. TABAK AND F. A. TAL, *Turbulent mixing of stratified flows*, Cubo Mat. Educ, 6 (2004).

[30] J. VIALARD AND P. DELECLUSE, *An ogcm study for the toga decade. part i: Role of salinity in the physics of the western pacific fresh pool*, J. Phys. Oceanogr., 28 (1998), pp. 1071–1088.

